JOURNAL OF PROPULSION AND POWER
Vol. 14, No. 2, March–April 1998

Aerodynamics Performance Prediction of Thrust-Vectoring Nozzles

A. Matesanz,* A. Velázquez,† and M. Rodríguez‡
SENER, 28760 PTM Tres Cantos, Madrid, Spain

This paper deals with a study that has been undertaken to analyze the aerodynamics performance of thrust-vectoring nozzles from an engineering design point of view. The rationale for the study is the existence of a trend within the aeronautics industry to provide fighter aircraft with thrust-deflection capabilities. Regarding practical design, and taking into account the fact that these nozzles have additional degrees of freedom, efficient prediction methodologies are needed to analyze the aerodynamics behavior associated with the many combinations of parameters that characterize these propulsive devices. The methodology presented is based on a combination of theoretical analysis and computational fluid dynamics in such a way that numerical simulation provides data which, after some theoretical work, are shaped in the fashion of generic design curves ready for use with practical problems. Details of the flow solver as well as a summary of its validation campaign are also provided.

Nomenclature

A_8 = geometric throat area, m^2
A_9 = geometric exit area, m^2
C_D = discharge coefficient, ratio between the actual and ideal mass flow
C_D^* = discharge coefficient for axisymmetric choked nondeflected nozzle
C_V = thrust coefficient, ratio between actual and ideal thrust
$C_{V\text{peak}}$ = maximum thrust coefficient for given nozzle geometry
c_p = specific heat at constant pressure, m^2/s^2 K
c_v = specific heat at constant volume, m^2/s^2 K
F = gross thrust, N
F_i = ideal gross thrust, N, Eq. (6)
k = turbulent kinetic energy, m^2/s^2
NPR = nozzle pressure ratio P_0/P_a
NPR_{peak} = NPR corresponding to $C_{V\text{peak}}$
P_a = ambient pressure, Pa
P_0 = total pressure at nozzle entry, Pa
R_g = gas constant, m^2/s^2 K, $c_p - c_v$
T_0 = total temperature at nozzle entry, K
W = nozzle mass flow, kg/s
W_i = ideal mass flow, kg/s, Eq. (2)
α = convergent petal angle, deg
β = divergent petal angle for nondeflected nozzle, deg
γ = specific heat ratio c_p/c_v
δ_e = effective thrust-vectoring angle, deg
δ_g = geometric thrust-vectoring angle, deg
ε = turbulent kinetic energy dissipation rate, m^2/s^3

Received May 6, 1997; revision received Oct. 16, 1997; accepted for publication Oct. 20, 1997.

*Fluid Mechanics Engineer, Aerospace Division; also Ph.D. Student at Madrid Carlos III University, 28911 Leganes-Madrid, Spain. Member AIAA.

†Fluid Mechanics Engineer, Aerospace Division; also Associate Professor, Mechanical Engineering Department, Madrid Carlos III University, 28911 Leganes-Madrid, Spain.

‡Fluid Mechanics Engineer, Aerospace Division; also Professor, Thermo-Fluid Dynamics Department, Madrid UPM University, 28040 Madrid, Spain.

Introduction

THE use of thrust-vectoring capabilities for fighter aircraft is becoming increasingly fashionable because of the benefits that can be obtained after the actual implementation of such propulsive devices.[1] Broadly speaking, there are two basic areas that are affected in a positive way whenever thrust direction is controlled: 1) combat maneuverability is greatly enhanced and 2) aircraft operations, such as those associated with takeoff and landing, become more efficient because of less demanding speed requirements. Reduction on drag can also be achieved because of the possibility of reducing vertical fins surface.[2]

To the authors' knowledge the German ballistic missile V-2 was the first vehicle to incorporate control vanes in the rocket jet. From that time up to now, many different concepts have been proposed, tested, and studied, most of them dealing with the utilization of more or less complex mechanical systems to achieve flow deflection without giving rise to unacceptable performance losses. Secondary flow injection, normal to the mainstream, has been proposed as a simple and straightforward way to change flow direction without having to resort to the use of moving parts. Restricting ourselves to mechanical systems, vanes immersed in the exhaust jet, and rectangular, axisymmetric, and spherical nozzles are configurations that have been studied in detail.

Macardle and Esker[3] analyzed vane nozzle performance and, although the mechanical design is rather simple, they reported large losses as a result of the internal flow structure. Rectangular two-dimensional nozzles were studied in great detail by NASA during the 1980s.[4,5] These nozzles, which are characterized by their pitch and yaw vectoring capabilities, were experimentally tested for a wide range of conditions and their performance coefficients are available in the literature. Spherical nozzles[6,7] are very attractive because of their compact design, good integration, reduced weight, and capability to achieve large deflections with comparatively small losses. However, their mechanical design is complex and the actuation system in particular has rather demanding requirements.

Axisymmetric thrust-vectoring nozzles represent a practical approach to the engineering problem. On one hand, these nozzles may not be as efficient as spherical ones, but their mechanical design is far more simple; on the other hand, these vectoring nozzles are not as simple as rectangular nozzles, but they do not have flow problems associated with the transition between circular and rectangular sections and the separation

extent is smaller because of geometrical constrains.[8] Most important, these nozzles are able to easily fit into existing fighter aircraft, which is a key issue for potential customers. Experimental testing of this type of nozzle has been reported by Carson and Capone[9] and Wing.[10] Relevant to this field, basic flow physics issues, such as the unsteady effects associated with a supersonic flow moving past a turning compression ramp, have also been studied.[11]

Because of the fact that convergent–divergent axisymmetric thrust-vectoring nozzles have more degrees of freedom than fixed geometry nozzles, engineering optimization of their aerodynamic performance requires the fine-tuning of a larger number of parameters. Therefore, in this case, it is very important to have reliable prediction tools that have undergone an extensive validation campaign, and that can efficiently sweep through multidimensional maps of design parameters. This paper presents a design methodology for axisymmetric convergent–divergent thrust-vectoring nozzles built upon the methodology developed and reported for fixed-geometry nozzles.[12] In that work, theory and experiments were combined to obtain generic correlations useful for practical engineering design purposes. The goal was to address the generation of an efficient prediction methodology for three-dimensional thrust-vectoring nozzle aerodynamic performance behavior by using computational fluid dynamics (CFD) instead of test bench results as a means of gathering the required data. In this regard, it is the opinion of the authors that, from the industrial standpoint, CFD yields maximum benefits when used to generate results that can be further generalized and shaped in the fashion of generic design curves to be used as a practical prediction methodology as opposed to its use as single-point analysis technique.

The work presented hereafter is organized as follows: 1) a description of the numerical code used to generate three-dimensional deflected flow data is given, 2) the methodology and the results obtained for convergent–divergent thrust vectoring nozzles are presented, and 3) conclusions are drawn.

Description of the Numerical Code

The three-dimensional CFD code developed to target these propulsive flows uses the finite element method. The numerical scheme has been evolved after the Streamline Upwind Petrov Galerkin (SUPG) method proposed by Hughes and Tezduyar[13]; specific details about the basic integration scheme are provided by Matesanz et al.[8,14,15] and Jimenez et al.[16] The algorithm results in an explicit time-marching solution procedure where increments of variables are calculated at each time iteration by using the weak formulation of Navier–Stokes equations. Local time stepping has been implemented to accelerate convergence in steady-state calculations. Space discretization, which is second-order accurate, is performed by means of trilinear hexahedra and integrals are performed by reduced integration in every element. Time derivatives are approximated by explicit time stepping with lumping of the mass matrix. To enhance stability of the numerical procedure, the following terms have been implemented into the algorithm: 1) lapidus artificial diffusivity, which smoothes streamwise gradients; 2) fourth-order dissipation term to damp high-frequency errors; 3) implicit residual smoothing; and 4) sock-capturing terms of the pressure switch type to improve resolution in shock-wave regions.

The code that has been developed is a Reynolds-averaged Navier–Stokes (RANS) version, where the user can choose between three different turbulence models: 1) algebraic, 2) k-ε, and 3) combined algebraic/k-ε. Even though the results of the validation campaign have been published in the previously mentioned references,[8,14–16] a summary of the main results is presented in the Appendix.

Prediction Methodology for Nondeflected Nozzles

To avoid misunderstandings with regard to the definition of the performance coefficients, this section starts by presenting the conventions used through this paper.

C_D is defined as the ratio between the actual and the ideal mass flow; that is,

$$C_D = W/W_i \tag{1}$$

where W_i corresponds to that of a convergent nozzle having the same throat area, NPR, and total temperature

$$W_i = A_8\sqrt{\gamma P_0^2/R_g T_0}\, f(P_0/P_a) \tag{2}$$

where the function $f(P_0/P_a)$ is

$$f\left(\frac{P_0}{P_a}\right) = \left(\frac{2}{\gamma+1}\right)^{(\gamma+1)/[2(\gamma-1)]} \tag{3}$$

if $P_0/P_a \geq [(\gamma+1)/2]^{\gamma/(\gamma-1)}$, and

$$f\left(\frac{P_0}{P_a}\right) = \sqrt{\frac{2}{\gamma-1}\left(\frac{P_a}{P_0}\right)^{(\gamma+1)/\gamma}\left[\left(\frac{P_0}{P_a}\right)^{(\gamma-1)/\gamma} - 1\right]} \tag{4}$$

if $P_0/P_a < [(\gamma+1)/2]^{\gamma/(\gamma-1)}$.

C_V is defined as the ratio between the actual and the ideal gross thrust

$$C_V = F/F_i \tag{5}$$

The ideal gross thrust is defined here as

$$F_i = W\sqrt{2c_p T_0[1 - (P_0/P_a)^{-(\gamma-1)/\gamma}]} \tag{6}$$

that corresponds to the ideal gross thrust of a convergent–divergent nozzle that expands the flow down to the ambient pressure. C_D determines the effective throat area and it is used to match engine cycle at design and off-design conditions, while C_V yields the gross thrust available at each flight condition.

In an axisymmetric convergent–divergent choked nozzle without deflection, the discharge coefficient depends on the convergent petal angle, and this particular value of C_D is called C_D^*. The thrust coefficient depends on NPR, exit-to-throat area ratio, specific heat ratio and, also, to a lesser extent, on the convergent petal angle. In an axisymmetric convergent–divergent nozzle, there is a specific value of NPR, $\mathrm{NPR}_{\mathrm{peak}}$, for which the C_V reaches its maximum, $C_{V\mathrm{peak}}$. The $C_{V\mathrm{peak}}$ value is only a function of the geometry ($A_9/A_{8\max}$, A_9/A_8, and $\boldsymbol{\beta}$), while $\mathrm{NPR}_{\mathrm{peak}}$ depends on γ. The maximum value of the thrust coefficient corresponds to a nozzle expanding to ambient pressure. The functional dependence (performance curves) of $C_{V\mathrm{peak}}$, $\mathrm{NPR}_{\mathrm{peak}}$, and C_D^* for a broad family of convergent–divergent nondeflected nozzles having a sharp throat has been determined in the past. Specific details are given by Rebolo et al.[12]

Prediction Methodology for Thrust-Vectoring Nozzles

When the nozzle is deflected (Fig. 1) the analysis grows more complicated because, in this case, both discharge and thrust coefficients depend on δ_e, which, in turn, depends on δ_g. In what follows, the prediction methodology for these propulsive devices is presented and validated by comparing with the experimental results given by Carson and Capone.[9]

First of all, experimental and CFD discharge coefficients have been plotted vs ($\delta_g - \boldsymbol{\beta}$) for different throat-to-exit area ratios A_9/A_8 and petal lengths. It happens that for typical values of A_9/A_8 ranging from 1 to 1.5, all normalized discharge coefficients collapse into a single curve (Fig. 2). Based on physical grounds and whenever the minimum area is smaller than A_8, which is the case for $\delta_g - \beta > 0$, the ratio $C_D(\delta_g)/C_D^*$ depends on δ_g and β separately. However, if the minimum area

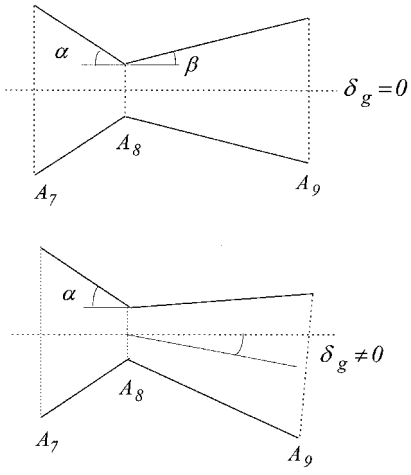

Fig. 1 Geometric parameters of the thrust-vectoring nozzle.

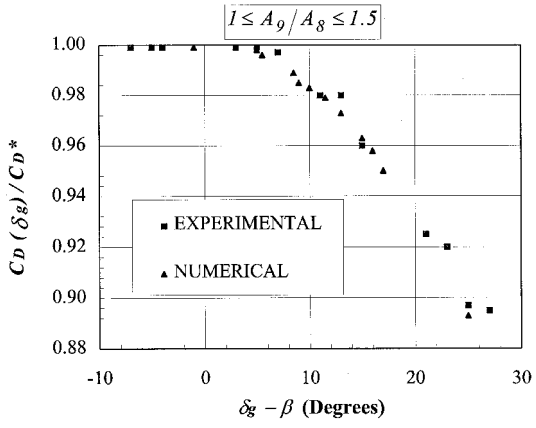

Fig. 2 Experimental vs CFD results for the discharge coefficient.

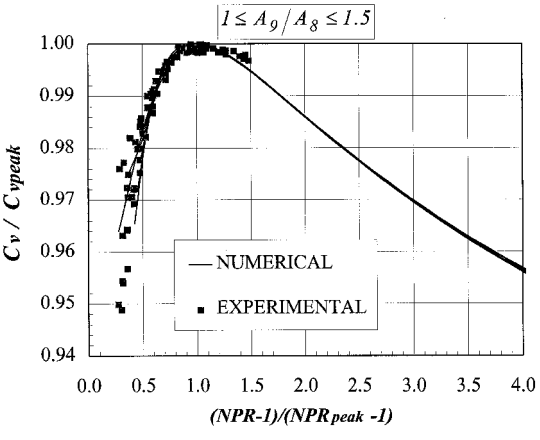

Fig. 3 Scaling for the thrust coefficient; experimental and numerical results.

section and A_8 share the same geometric layout, for instance, they both have a circular shape, the first-order dependence is on $(\delta_g - \beta)$. This is the reason why, for the cases studied through this work, that the dependence of $C_D(\delta_g)/C_D^*$ on β alone, which is of the second order and probably smaller than the uncertainty associated to the data being used, was not detected.

Concerning the thrust coefficient, it was found that the appropriate correlating parameter for $C_V/C_{V\text{peak}}$ is (NPR − 1)/(NPR$_{\text{peak}}$ − 1), where $C_{V\text{peak}}$ and NPR$_{\text{peak}}$ correspond to the deflected nozzle. Furthermore, we found out that a quite accurate estimate is obtained for these two parameters by using the nondeflected nozzle functions with an effective exit-to-throat area ratio of $A_9/(A_8 \cdot C_D)$. As can be readily observed in Fig. 3, experimental and CFD results lay very close to a single curve for values of this parameter larger than 0.5. Discrepancies in the low NPR regime are sequentially caused by internal shock-wave structure, flow separation at the throat, and subsonic regime.[17] The correlation presented in Fig. 3, which allows for the knowledge of the gross thrust but not for its direction, is universal in the sense that it holds for different values of the throat area, exit-to-throat area ratio, petal lengths, and deflection angle.

Detailed analysis of the results show that normalized thrust deflection also correlates with the same parameter (NPR − 1)/(NPR$_{\text{peak}}$ − 1), as seen in Fig. 4, where

$$\phi = 1 + \frac{1}{2}\varsigma\left(\frac{A_9}{A_8}\right)\left\{1 + \tanh\left[\frac{2}{3}\left(\frac{\text{NPR} - 1}{\text{NPR}_{\text{peak}} - 1} - \frac{5}{2}\right)\right]\right\} \tag{7}$$

$$\varsigma\left(\frac{A_9}{A_8}\right) = 0.2778 - 0.1984\frac{A_9}{A_8}, \quad \text{valid for} \quad 1 \le \frac{A_9}{A_8} \le 1.5 \tag{8}$$

Function ϕ comes into play because it has been observed that larger A_9/A_8 yields more efficient flow deflection for large NPRs. The single design curve for the normalized thrust deflection does not hold for values of (NPR − 1)/(NPR$_{\text{peak}}$ − 1) smaller than approximately 0.5. The reason, as in the case of the thrust coefficient, is that for low-pressure ratios, the shock waves that form in the divergent part of the nozzle cause the flow to separate in the vicinity of the wall. It is the extent of

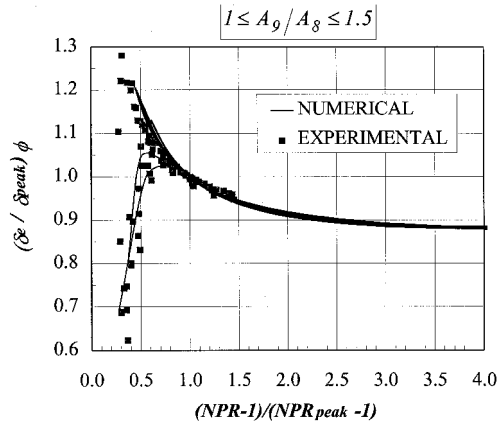

Fig. 4 Scaling for the effective deflection angle; experimental and numerical results.

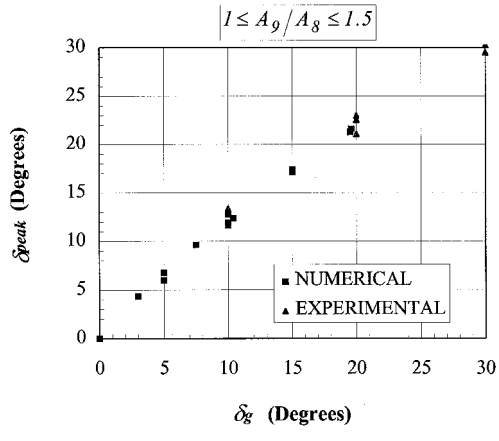

Fig. 5 δ_{peak} as a function of δ_g.

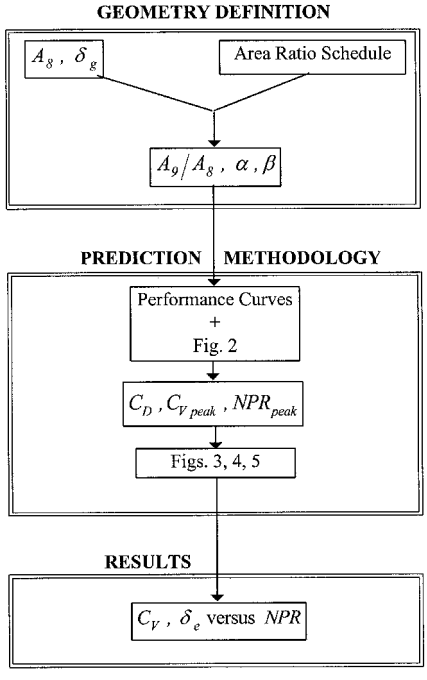

Fig. 6 Block diagram for the prediction methodology.

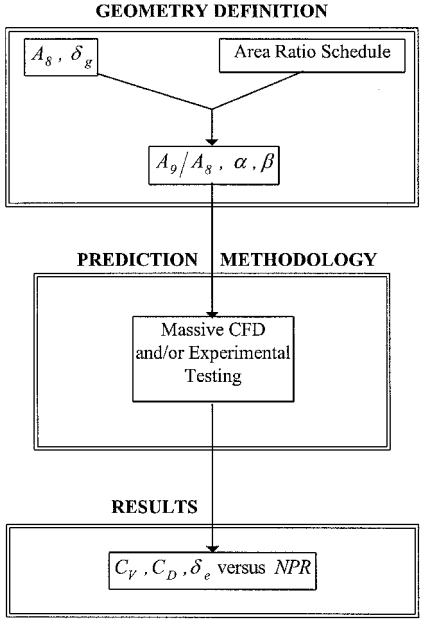

Fig. 7 Alternative prediction methodology.

this separation, the one that determines the branch (Fig. 4), on which the nozzle working point stands. If the separation is small, normalized thrust deflection is large (upper branch); on the contrary, if separation grows significant, thrust deflection drops dramatically (lower branch). Finally, δ_{peak} as a function of δ_g is shown in Fig. 5.

To summarize the methodology being presented, a block diagram showing the steps to be undertaken in real design problems is given in Fig. 6. First of all, the specific area ratio schedule of the nozzle defines A_9/A_8, α and β as a function of A_8 and δ_g. Then the discharge coefficient of the deflected nozzle is taken from the design curve given in Fig. 2. This value is used to obtain $C_{V\text{peak}}$ and NPR_{peak} from the performance curves by means of an appropriate scaling, $A_9/(A_8 \cdot C_D)$. At this point, design curves given in Figs. 3–5 can be readily used to get the values of both thrust coefficient and effective thrust-vectoring angle as a function of the nozzle pressure ratio. Working in this way it is straightforward to make the systematic parametric analysis of a given thrust-vectoring nozzle provided that it belong to a certain family; namely, that it has a sharp throat and that $1 \leq A_9/A_8 \leq 1.5$.

The other way around the problem (Fig. 7) would be to undertake a massive CFD and/or experimental campaign to assess the aerodynamics coefficients of the nozzle. However, we believe that, in this case, the time needed to produce results would certainly offset the benefits associated to the, probably marginal, increments in accuracy. It is the experience of the authors that the time invested in the generalization of the results by means of generating design curves, certainly pays off when the actual engineering problem is addressed and reliable answers have to be provided within short time spans.

Conclusions

A prediction methodology has been generated for the study of the aerodynamics performance of thrust-vectoring nozzles. An extensive three-dimensional numerical simulation campaign has been undertaken not to analyze specific configurations but to use the CFD data for the generation of generic design curves that can be used in practical design problems. It has been found out that by using an appropriate scaling, design curves can be obtained for the critical aerodynamics parameters such as discharge and thrust coefficients and effective deflection angle. The methodology that has been presented is built upon an existing one for nondeflected nozzles. Experimental data available in the literature have also been used to check the validity of the correlations that were obtained.

Finally, it can be concluded that concerning practical engineering design applications in this field, it is possible to generalize results obtained from CFD and/or experimental tests for its use as a time-saving and accurate prediction tool.

Appendix: Code Validation

This Appendix contains the results of the validation campaign that was undertaken to validate the CFD solver used to gather the required data for generating a prediction methodology for thrust-vectoring nozzles.

Validation Case 1

A one-eighth-scaled convergent–divergent axisymmetric nondeflected nozzle was tested in cold flow conditions in a test bench with the following parameters: exit-to-throat (nonde-

Table A1 Aerodynamic coefficients

Results	C_V	C_D
Numerical	0.989	0.941
Experimental	0.988	0.947

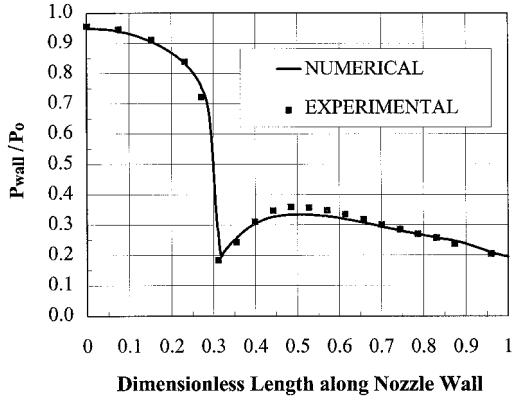

Fig. A1 Experimental vs numerical static pressure distribution along the nozzle walls.

flected) area ratio = 1.26, entrance-to-throat area ratio = 2.00, and NPR = 5.00.

Table A1 shows the comparison, in terms of aerodynamic coefficients, between the experimental and numerical results obtained using a grid having 121,440 elements, while Fig. A1 plots the predicted static pressure distributions vs the data measured on the nozzle wall at the test bench. The agreement is quite reasonable even at the large expansion occurring at the sharp throat.

Validation Case 2

The code that has been developed has a RANS version where the user can choose between three different turbulence models: 1) algebraic, 2) k-ε, and 3) combined algebraic/k-ε. First, the experimental results on film cooling with injection normal to a flat plate provided by Papell[18] were used for comparison. The following set of conditions were considered: injection angle = 90 deg, main flow Mach number = 0.52, main mass flow = 5.432 kg/s, cooling mass flow = 0.079 kg/s, main flow velocity = 290 m/s, cooling velocity = 84.6 m/s, main flow temperature = 833 K, and cooling temperature = 456 K.

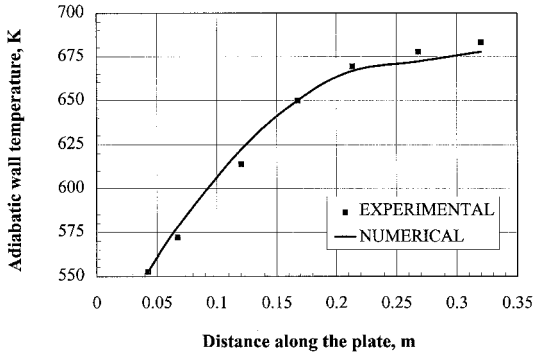

Fig. A2 Experimental vs numerical adiabatic wall temperature results downstream of the cooling injection in a flat plate.

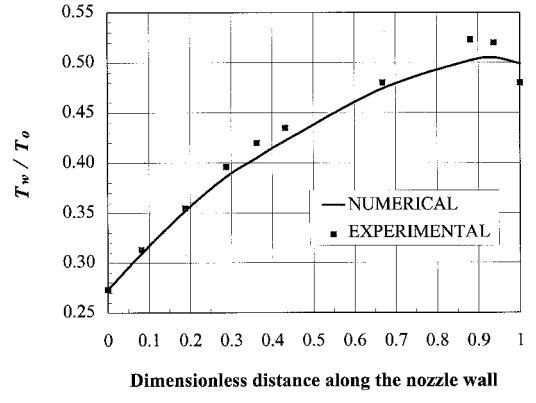

Fig. A3 Experimental vs numerical adiabatic wall temperature results downstream of the cooling injection in the nozzle.

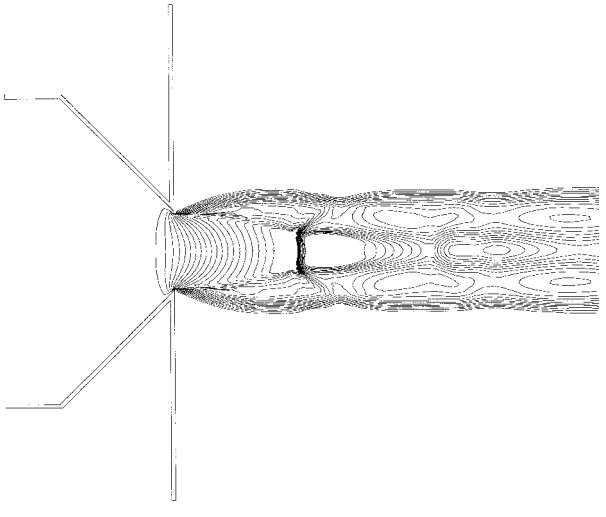

Fig. A4 Jet flow structure with nonregular reflection (Mach disk).

Table A2 Mach disk size

	NPR		
Results	6	7	8
Numerical	0.33	0.40	0.56
Experimental	0.31	0.44	0.54

Table A3 Mach disk axial position

	NPR		
Results	6	7	8
Numerical	3.08	3.38	3.48
Experimental	3.18	3.44	3.68

Figure A2 shows the comparison between CFD and experimental results. The maximum deviation on adiabatic wall temperature is less than 10%.

To test code accuracy in a somewhat more realistic geometry a dedicated experimental setup was again prepared. It consisted of a one-eighth-scaled axisymmetric convergent-divergent nozzle having slot film cooling injection according to the following parameters: injection angle = 15 deg forward, main mass flow = 1.70 kg/s, cooling mass flow = 0.13 kg/s, main flow temperature = 1200 K, cooling temperature = 300 K, and nozzle pressure ratio = 3.7.

Figure A3 shows the comparison between CFD and experimental results with regard to adiabatic wall temperature along the divergent part of the nozzle. The sudden temperature drop at the far end of it is generated by external air ingestion. It can be observed that, out of this particular zone, discrepancies are less than 2%.

Validation Case 3

In the first two validation cases, only wall variables, such as pressure and temperature, were used for comparison. Therefore, the question remained as to how the code can predict generic flow structures. This is the reason why a third validation effort took place with the aim of predicting Mach disk radius and location in jet flows downstream of a convergent nozzle. The experimental study of Addy[19] was used as the benchmark for comparison purposes. A sharp-edged 45-deg convergent nozzle, supplied with air at a stagnation pressure of 725 kPa was tested at three different NPRs: 6, 7, and 8. Figure A4 shows an overview of the Mach number distribution in the flowfield, where the Mach disk can be distinctly seen. Tables A2 and A3 give the comparison between CFD and experimental results regarding the Mach disk size and its location.

Acknowledgment

The authors are grateful to M. Valls, Director of the Department of Aeronautics at SENER, for his continuous support.

References

[1]Benjamin, G.-O., *Vectored Propulsion, Supermaneuverability and Robot Aircraft*, Springer–Verlag, New York, 1990.

[2]Loria, C. J., Kelly, M., and Hatney, R., "X-31 A Quasi-Tailless Evaluation," *IEEE Aerospace Applications Conference*, Inst. of Electrical and Electronics Engineers, Vol. 4, New York, 1996, pp. 253–276.

[3]Macardle, J. G., and Esker, B. S., "Performance Characteristics of a Variable-Area Vane Nozzle for Vectoring an ASTOVL Exhaust Jet up to 45 Degrees," AIAA Paper 93-2437, June 1993.

[4]Re, R. J., and Leavitt, L. D., "Static Internal Performance Including Thrust Vectoring and Reversing of Two-Dimensional Convergent-Divergent Nozzles," NASA TP-2253, Feb. 1984.

[5]Taylor, J. G., "Static Investigation of a Two-Dimensional Convergent-Divergent Exhaust Nozzle with Multiaxis Thrust-Vectoring Capability," NASA TP-2973, April 1990.

[6]Maclean, M. K., and Meyer, B. E., "Scale Model Test Results for Several Spherical Two-Dimensional Nozzle Concepts," AIAA Paper 93-2430, June 1993.

[7]Cler, D. L., Mason, M. L., and Guthrie, A. R., "Experimental Investigation of Spherical Convergent-Flap Thrust-Vectoring Two-Dimensional Plug Nozzle," AIAA Paper 93-2431, June 1993.

[8]Matesanz, A., Velázquez, A., and Rodríguez, M., "Numerical Study on Some Fluid Dynamics Aspects of Axisymmetric Thrust Vectoring Nozzles," AIAA Paper 94-3365, June 1994.

[9]Carson, G. T., and Capone, F. J., "Static Internal Performance of an Axisymmetric Nozzle with Multiaxis Thrust-Vectoring Capability," NASA TM-4237, Feb. 1991.

[10]Wing, D. J., "Performance Characteristics of Two Multiaxis Thrust-Vectoring Nozzles at Mach Number up to 1.28," NASA TP-3313, May 1993.

[11]Park, S. O., Chung, Y. M., and Sung, H. J., "Numerical Study of Unsteady Supersonic Compression Ramp Flows," *AIAA Journal*, Vol. 32, No. 1, 1994, pp. 216–218.

[12]Rebolo, R., Arredondo, P., Matesanz, A., Velázquez, A., and Rodríguez, M., "Aerodynamic Design of Convergent-Divergent Nozzles," AIAA Paper 93-2574, June 1993.

[13]Hughes, T. J. R., and Tezduyar, T. E., "Finite Element Methods for First-Order Hyperbolic Systems with Particular Emphasis on the Compressible Euler Equations," *Computer Methods in Applied Mechanics and Engineering*, Vol. 45, 1984, pp. 217–284.

[14]Matesanz, A., Velázquez, A., and Rodríguez, M., "Mach Disk Simulation in Jets from Convergent-Divergent Axisymmetric and Thrust Vectoring Nozzles," AIAA Paper 94-2328, June 1994.

[15]Matesanz, A., Velázquez, A., and Rodríguez, M., "Numerical Simulation of Slot Film Cooling in Convergent-Divergent Nozzles," AIAA Paper 93-1977, June 1993.

[16]Jimenez, A., Esteban, A., Matesanz, A., Velázquez, A., and Rodríguez, M., "Turbulence k-ε Models in the Study of Supersonic External Flows," AIAA Paper 96-4586, Nov. 1996.

[17]Kuchar, A. P., "Variable Convergent-Divergent Exhaust Nozzle Aerodynamics," edited by G. Oates, Air Force Aero Propulsion Lab., TR-78-52, July 1978.

[18]Papell, S., "Effect on Gaseous Film Cooling of Coolant Injection Through Angled Slots and Normal Holes," NASA TN D-299, Sept. 1960.

[19]Addy, A. L., "Effect of Axisymmetric Sonic Nozzle Geometry on Mach Disk Characteristics," *AIAA Journal*, Vol. 19, No. 1, 1981, p. 121.